1992

Mass Dependent Loss of Resolution in Radially Inhomogeneous ExB Ion Traps

Mark A. Capron
University of Northern Iowa

Susan S. Haskin
University of Northern Iowa

Curtiss D. Hanson
University of Northern Iowa

Mass Dependent Loss of Resolution in Radially Inhomogeneous ExB Ion Traps

MARK A. CAPRON, SUSAN S. HASKIN and CURTISS D. HANSON

University of Northern Iowa, Department of Chemistry, Cedar Falls, IA 50614-0423

ExB ion traps, such as Fourier transform Ion Cyclotron Resonance mass spectrometers (FT-ICR), mass analyze sample ions based on differences in their cyclotron frequencies in a homogeneous magnetic field. The high resolution mass measurements of FT-ICR are based on the relationship between the frequency of the cyclotron orbit and the mass-to-charge (m/q) ratio of an ion. Both the orbit and the frequency/mass relationship result from the radial forces on the ion. Ions trapped by inhomogeneous electric fields experience different magnitudes of the radial electric fields at different positions resulting in a positionally dependent frequency. Such differences in orbital frequencies for ions of a single m/q ratio result in line broadening and loss of resolution.
INDEX DESCRIPTORS: Ion cyclotron resonance, mass spectrometry, ion motion, loss of resolution

Since the early 1970's, technological advances have led to the development of a number of different instruments for mass spectrometric analysis. These new generation mass spectrometers have increased the sensitivity and versatility of the technique by trapping ions in quadrupolar electric (1,2,3,4) or crossed electric and magnetic fields (5,6,7). Localization of atomic particles in an ion trap permits a variety of structural probes to be used to characterize and quantify the sample (8,9). The versatility of an ion trap makes it a valuable technique for mass spectrometry (MS) studies in both academic and industrial settings.

Penning ion traps store and analyze ions by superimposing an electrostatic potential perpendicular to a uniform magnetic field (ExB fields) (10). The ExB geometry provides the basis for the Fourier transform ion cyclotron resonance mass spectrometers (FT-ICR) (11), which separate and measure sample ions of different masses based on differences in their cyclotron frequencies in a homogeneous magnetic field. The analytical utility of FT-ICR can be attributed to the performance characteristics created by the Fourier analysis [e.g., sensitivity (12), mass resolution (13), mass range (14), multichannel advantage (15), and the versatility of the instrument for various ionization methods (16)]. In addition to the ultra-high resolution and simultaneous ion detection over a wide mass range, a large thrust in the research surrounding Fourier compatible mass analysis has emphasized detection and high resolution at high mass (17). However, results in high mass analysis indicate that a non-theoritical loss of resolution exists for high mass ions injected from external ion sources. In order to realize the potential of FT-ICR, it is important to investigate mass dependent mechanisms for loss of resolution.

Ion detection in FT-ICR is achieved by observing an induced image current resulting from the orbital motion of an ion ensemble. The orbital motion is established due to the equilibrium between the radial forces acting on the ion. An ion in a magnetic field is affected by the Lorentz force of the magnetic field and the centrifugal force. The equilibrium can be expressed as:

$$\frac{mv^2}{r} = qvB$$
$$r = \frac{mv}{qB}$$

$$(1)$$

where v is the velocity of the ion perpendicular to the magnetic field, B is the magnetic field strength, and r is the resultant orbital radius. From this relationship, the angular frequency of the orbit (w_c) in a static magnetic field is shown to be solely dependent upon the m/q ratio of the ion.

$$\omega_c = \frac{v}{r} = \left(\frac{q}{m}\right)B$$

$$(2)$$

Following ion formation and rf excitation, detection occurs in the confines of a perpendicular electric field (ExB) that traps the ion population in the region of the detection electrodes. The resultant potential well results in a oscillatory motion of the charged particles along the axis of the magnetic field. The motion of ions trapped in the confines of a homogeneous ExB trap is a combination of the natural cyclotron (orbital) motion superimposed on a harmonic trapping oscillation resulting in a helical trajectory.

Imperfect electric fields having vector components parallel ($E_\parallel$) to the magnetic field introduce a new radial force ($qE_\parallel$). This new force, shifts the measured radial frequency by a factor dependent upon the ion's velocity and magnitude of $E_\parallel$.

$$qvB = \frac{mv^2}{r} + qE_\parallel$$

$$\omega_c = \frac{v}{r} = \frac{q}{m}\left(B - \frac{E_\parallel}{v}\right)$$

$$(3)$$

In a cubic trap utilizing induced image current as a detection scheme, all ions must be accelerated to the same radius for detection regardless of m/q ratio. At the detection radius, high mass ions will have lower velocities than low mass ions (Equation 1). Therefore, the frequency shift induced by the inhomogenous field will be larger for those ions having the high m/q ratio (Equation 3).

The frequency shifts resulting from ion interaction with the DC electric field can be corrected by use of calibration tables (18) only if all the ions of a given m/q ratio are shifted to the same frequency. When the electric field is homogeneous within the spatial dimensions of the ion packet, the radial force due to the DC electric field is the same for all ions of the packet. However, when the electric field is inhomogeneous (i.e., differnt values of $E_\parallel$ as a function of position) in the dimensions of the ion ensemble, the ions at different locations will experience different magnitudes of $E_\parallel$. Therefore, the inhomogeneous radial electric field causes differences in the orbital frequencies for spatially distributed ions of a single m/q value.

In addition, the inhomogeneities of the electric field produce a periodic drift of the center of the cyclotron orbit (19). The resultant epicycle (magnetron motion) has been shown to produce both frequency shifts and sidebands. The magnitude of the magnetron motion has been shown to be proportional to the m/q ratio and the $E_\parallel/B$ ratio.

Evaluation of mass dependent frequency shifts are further complicated by ExB fields that are both axially and radially inhomogeneous. As an ion moves through the cell, its frequency will be changed by the regional electric field. To address the issues concerning loss of mass resolution, it is necessary to evaluate the effect of an inhomogeneous DC electric field on an ion ensemble having a shifting spatial distribution.

EXPERIMENTAL

Electrostatic contours were calculated and displayed using the trajectory calculation program SIMION (*version 4.0*) (*20*) on a math co-processor equipped PC/AT type IBM compatible computer. SIMION is an electrostatic lens analysis program originally developed for mainframe computers by D.C. McGilvery at Latrobe University, Department of Physics and Chemistry, Bundoora Victoria, Australia. The SIMION/IBM-PC version was developed at the Idaho National Engineering Laboratory by D.A. Dahl and J.E. Delmore. SIMION allows placement of electrodes in a user defined array permitting user defined equipotential electric field lines to be calculated for the array. The array is used to define a pixel grid then the electrodes and field calculations are generated from the grid. This allows investigations pertaining to inhomogeneous electric fields and ion motion in a complicated ExB field to be evaluated in a systematic manner.

Electrostatic forces are calculated in terms of volts per grid unit. As the ion travels through the potential array it moves from ion square of the grid into another. The simion program assumes a sixteen point array for the grid unit. Voltage 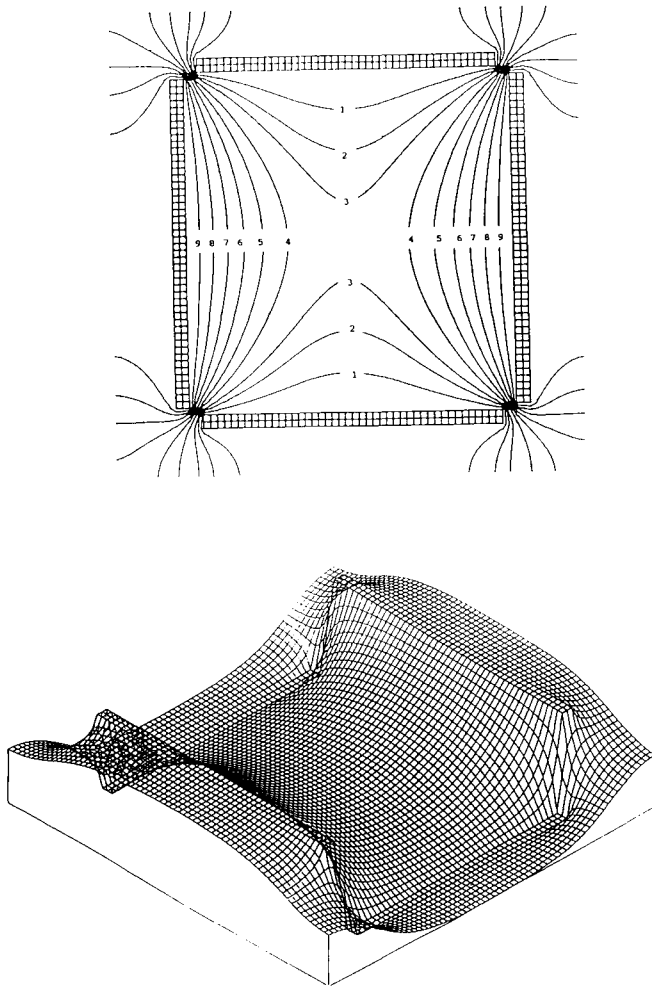gradients are calculated for the points which surround a specific ion's location in the potential array. The potential at each point is calculated via linear interpolation using the surrounding grid points. The linear interpolation is corrected if the grid unit the ion is located in is directly adjacent to an electrode surface. For adjacent electrodes the field is extrapolated from existing electrostatic field calculations.

Ion trajectories are calculated on the basis of the current ion location and velocity. The forces acting on the ion from the electric field (*and also magnetic fields*) are used to compute the current ion acceleration and used by numerical integration to predict the next position and velocity at the next time step. A standard fourth order Runge-Kutta method is used for the numerical integration of the ion's trajectory. This approach
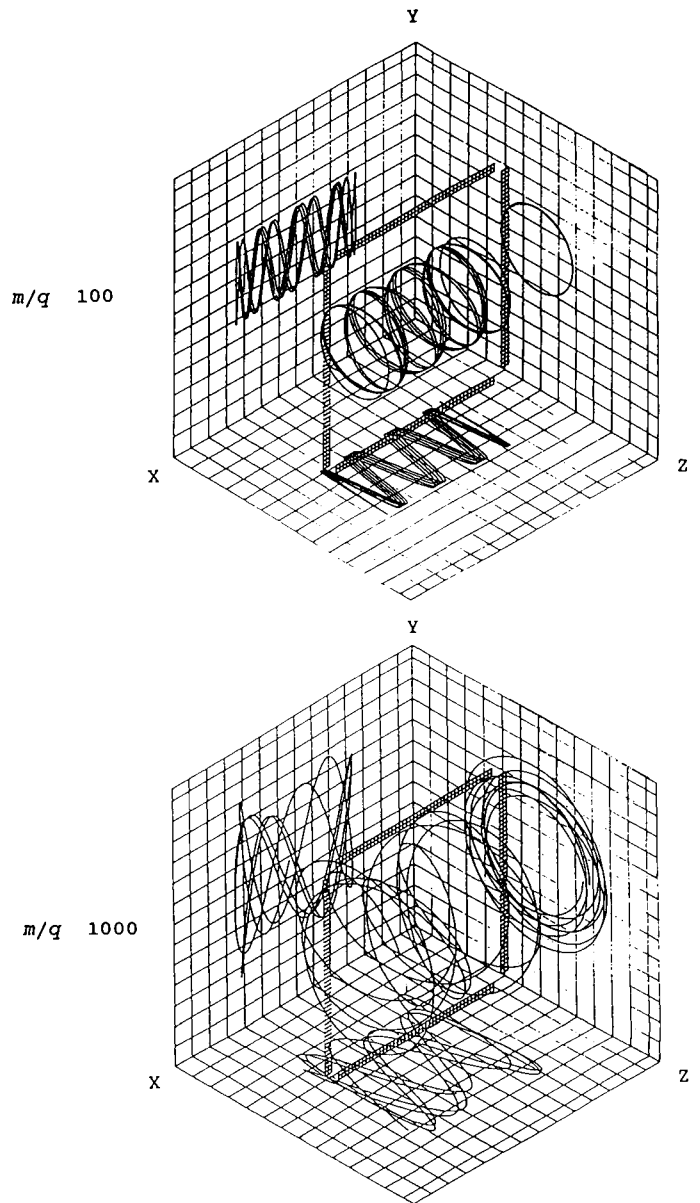

Fig. 1 (*Top*) Trapping plates are used to prevent ions from escaping along the magnetic field line. The trapping plates produce an electric field containing both parallel and perpendicular vector components (*i.e.,* *radially inhomogeneous*). (*Bottom*) The potential surface of X = 0 plane of the 10 V ICR cell used in the simulation.

Fig. 2. Three-Dimensional views of ion trajectories for m/q 100 (Top) and 1000 amu (bottom). The instantaneous velocity and position of the ions is recorded as a function of time to permit evaluation of the trajectories. The projection in the Y-Z plane illustrates the periodic drift of the orbit center (magnetron motion) as the m/q increases.
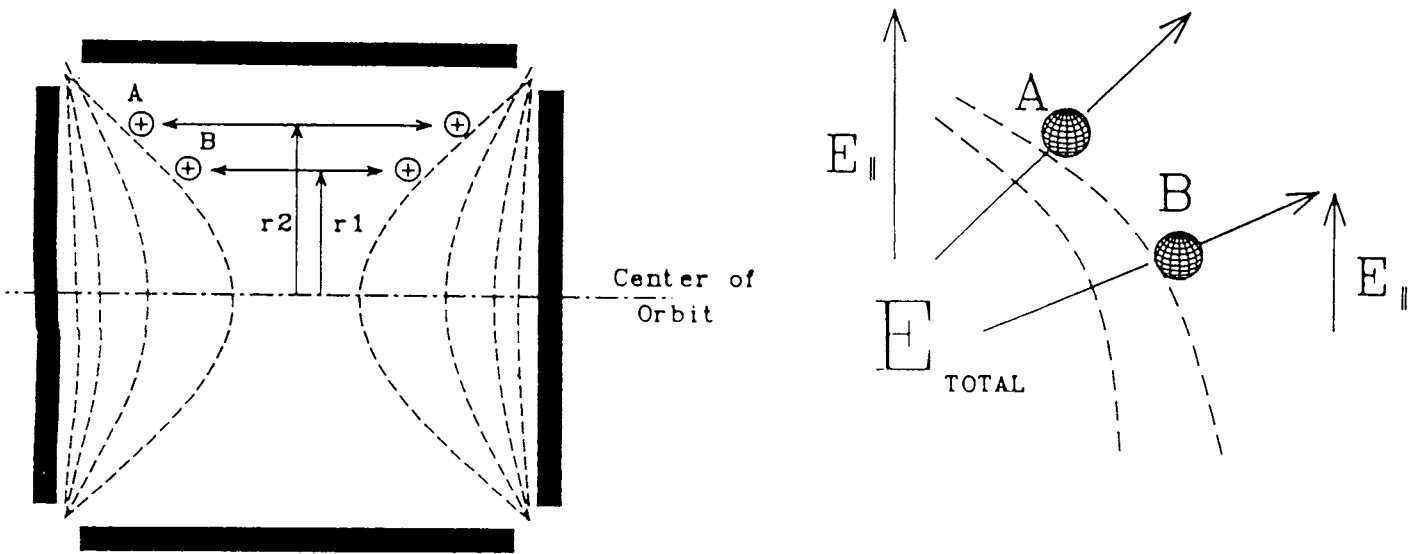
Fig. 3. Ions having different radii interact with different regions of the applied electric field. If the field is radially inhomogeneous, the ions will experience different magnitudes of $E_\parallel$.

has good accuracy and the ability to use continuously adjustable time increments.

The cell design consisted of parallel electrode plates generating an electric field perpendicular to a 3 Tesla magnetic field. A typical geometry for ExB ion traps are cubic cells comprised of six electrically isolated plates. Two plates orthoganal to the electrostatic trapping plates (*parallel to the magnetic field*) were held at a ground reference potential to create the simulated electromagnetic bottle. Figure 1 contains a plot of the electrostatic potential energy surface generated by placing 10 volts on the trap plates of an ion cell having cubic geometry. The radial component of the electric field in a cubic ICR cell is both axially and radially inhomogeneous. The ion location and kinetic energy is written to a file such that the impact of the electric field on the three dimensional ion trajectory can be evaluated. An example of the resulting trajectories for ions of m/q 100 and m/q 1000 confined in a 10 volt cubic trap are shown in Figure 2.

RESULTS AND DISCUSSION

The effect of the radial inhomogeneities is illustrated by considering the trapping field interaction on two ions having equal axial translational energies (*Z-axis*), but different radial velocities. A distribution of radial velocities corresponds to a spatial distribution in the X-Y plane (*Equation 1*). Illustrated in Figure 3 are the different electric field vectors acting on two ions having different radii. When the ions have different spatial positions, the magnitude of $E_\parallel$ experienced by the two ions is not the same, resulting in different radial frequencies. Differences in radial frequency for two ions of the same m/q ratio results in loss of resolution by two mechanisms: first, line broadening due to the multiple frequencies for a single m/q ratio, and second, frequency identification using Fourier transforms is dependent upon the length of time the signal is observed (*Equation 4*).

$$\frac{M}{\Delta M} \propto \frac{B}{m/q}\, t$$

(4)

The signal in FT-ICR can only be detected by the coherent (*i.e., in-phase*) motion of a large number of ions. Ions of the same m/q ratio having a multitude of frequencies results in a loss of the coherent motion by dephasing the ion population (*Figure 4*). Loss of the detected signal will then occur.

Contained in Figure 5 is a plot of the Y position as a function of time for ions of m/q 1000 having orbital radii of 5 and 7 mm. This initial separation is representative of the spatial distribution following excitation for ions injected into the ion trap. The frequencies of the two ions are significantly different due to the positionally dependent magnitude of $E_\parallel$. The difference in frequencies results in the loss of the coherent motion of the two ions and limits the duration of the time domain signal for the m/q 1000. The mass dependence of the dephasing rate is shown in Figure 6. This illustrates the more rapid loss of the time domain signal for high mass ions, however, the projected resolu-
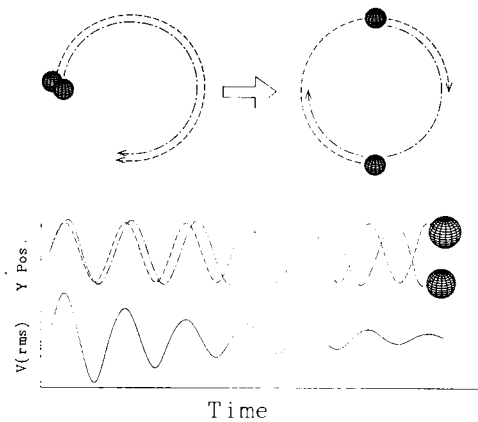

Fig. 4. The signal created from an induced image current is produced from the coherent motion of an ion population. Ions of the same m/q ratio having different frequencies will dephase as they approach a node in their beat frequency. The result of this is loss of the ion ensemble and ultimately the loss of detected signal.
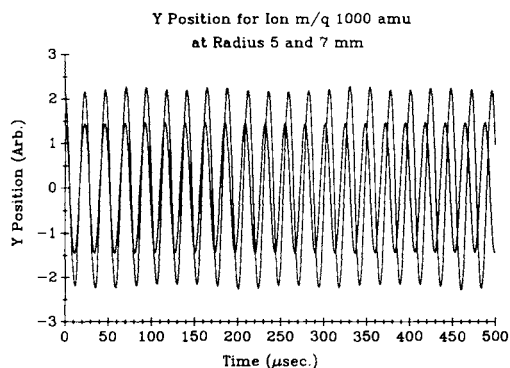
Fig. 5. The frequency of two ions having different radii can be evaluated by plotting Y-position as a function of time. The two distinct frequencies illustrates the loss of coherent ion motion.

tion loss solely from this effect is insufficient to explain the present limitations to high mass.

A secondary effect of the inhomogeneous electric field is the periodic drift of the center of the orbit or the magnetron motion (21). In original ICR drift cells, this motion was shown to dependent upon the m/q ratio of the ions and the $E_{\parallel}/B$ ratio. The magnitude of the drift theoretically increases with both $E_{\parallel}$ and m/q (22). The predicted mass dependance of the magnetron motion is illustrated by comparing the projection of the ion motion in the Y-Z plane for ions of m/q 100 and m/q 1000 in Figure 2.

The inhomogeneous electric field, causes $E_{\parallel}$ to be positionally dependent and, therefore, changes as the center of the ion's orbit drifts both axially and radially. The fluctuations in $E_{\parallel}$ result in continuous changes in radial frequency, axial frequency, and magnetron drift by reducing the effective force of the magnetic field.

$$B_{effective} = B - \frac{E_{\parallel}}{v} \tag{5}$$

where $E_{\parallel}$ inhomogeneities is the product of the applied trapping voltage, E_t, and a cell constant, ξ (23). Rearranging and substituting into Equation 4 results in mass resolution that is dependent upon the applied potential field and the cell design.

$$Resolution \propto \frac{[B - \frac{E_t \xi}{v}]}{m/q} t \tag{6}$$

The velocity of the ions in the cyclotron orbit can be obtained from Equation 1, where

$$v = \frac{B}{r}(q/m) \tag{7}$$

Combining Equations 6 and 7 at a constant radius of detection for all ions; which is determined by the cell constant, ξ, the result is Equation 8.

$$Resolution \propto \frac{[B - (m/q)(\frac{E_t \xi}{B})]}{m/q} t \tag{8}$$

From Equation 8, it can be seen that mass resolution is now not only more dependent upon the m/q ratio of the detected ions than previously predicted, but it can also be shown to be dependent upon the cell geometry and applied trapping voltage.

The impact of a continuously changing $E_{\parallel}$ on orbital frequency is shown in Figure 7. It is important to note that although an ion of m/q

100 effectively produces a single frequency (*1.3 ppm deviation as a function of time*), an ion of m/q 1000 produces a wide range of frequencies (*1.6x10⁴ ppm deviation as a function of time*) due to the changing magnitude of $E_{\parallel}$. The poor frequency definition corresponds to a loss of mass resolution for high mass ions. The resultant mass spectrum for these two trajectories can be simulated through Fourier analysis of Y position as a function of time (*i.e., the time domain spectrum*). Figure 8 is a simulated spectrum for ions of m/q 100 and m/q 1000 in a cubic trap [(*2.54 cm*)³] with 10 volts applied to the trapping plates. Note both the loss of resolution and the shift in the observed mass for the ions of m/q 1000.

CONCLUSIONS

The ability to perform high resolution mass measurements in FT-ICR is dependent upon two principle considerations: first, the duration of the time-domain signal and second, the relationship between orbital frequency and m/q ratio. For the case where ions are produced in the cell with low translational energies and a small spatial distribution, both considerations are fulfilled resulting in high mass resolution. Conversely, ion ensembles having a large spatial distribution following excitation experience both frequency and phase modulations in the confines of the cubic ICR cell. The loss of frequency definition results in peak broadening and termination of the time-domain signal. The inverse relationship between mass and velocity in a cyclotron radius increases the impact of inhomogeneous electric fields on high mass producing a limitation to high resolution, high mass analysis.

The problems of an inhomogeneous electric field are increased by the ionization methods used for high mass molecules. Ionization sources [*i.e., FAB (24), LD (25), SIMS (26), etc.*] capable of desorbing and ionizing large involatile and thermally labile biomolecules operate at high pressure (*ca. 1x10⁻² to 1x10⁻⁴ torr*). Such sources are incompatible with the ultra high vacuum conditions required for detection in FT-ICR. To overcome the problem of high pressure sources, ionization of biomolecules is done external to the detection region. Therefore, ions produced in the source must be given significant kinetic energy to move them from the source to the detection region. The impact of the kinetic energy is threefold. First, high radial kinetic energy results in a broad spatial distribution following excitation (27). Second, high trapping voltages (E_t) are required to trap ions that have high axial
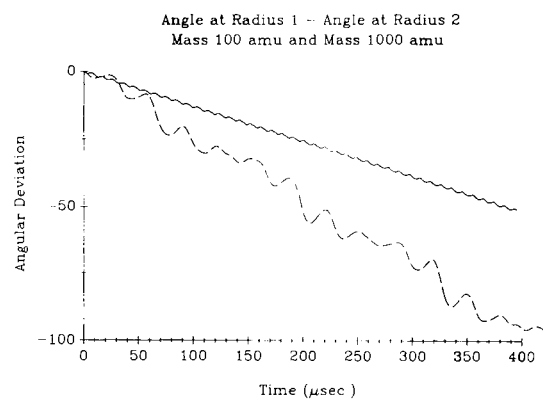

Fig. 6. The angular deviation of two ions (*m/q = 100 and m/q = 1000 amu*). This plot illustrates that ions of larger mass become more quickly dephased resulting in a mass dependent loss of coherence. This loss of coherence is represented by the rate of dephasing (*i.e. the slope of each plot*).
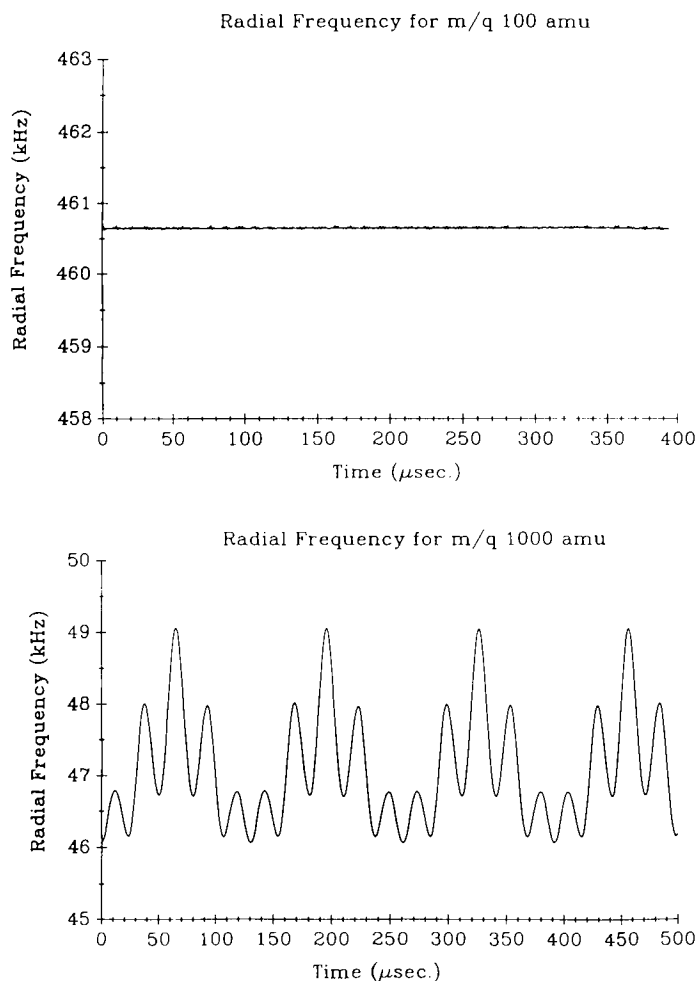
Radial Frequency for m/q 100 amu

Radial Frequency for m/q 1000 amu

Fig. 7. (*Top*) The radial frequency for *m/q* 100 amu is virtually unaffected by the electric field (*1.3 ppm deviation as a function of time*). (*Bottom*) The radial frequency for *m/q* 1000 amu illustrates the effect of the inhomogeneous electric field on high mass (*1.6x10⁴ ppm deviation as a function of time*). Both plots were made at a radius of 7 mm.

kinetic energy. As shown by Equation 8, when the trapping voltage increases, the obtainable mass resolution decreases. Finally, the image current induced in the receive electrodes is a function of the number of ions and the distance from the receive electrode. Low abundance ions suffer the worst effects because they must be accelerated to large radii in order to produce a detectable signal. For example, desorption of large involatile biomolecules in an external ion source results in a low abundance of molecular ions trapped in the ion cell relative to inorganic cluster ions or ions produced by electron impact inside the cell. Large molecules injected into the cell with high initial velocity results in a large spatial distribution following excitation. These ions must be accelerated to the extremes of the cell to produce a detectable signal resulting in phase and frequency modulations.

In order to realize the potential resolution for high mass ions in Penning experiments such as FT-ICR, it is essential that the kinetic energy used to inject ions produced in external ion sources be reduced so that E_t can be reduced. Furthermore, new cell designs which reduce the electric field inhomogeneities should be designed (*28, 29, 30, 31*) and utilized.

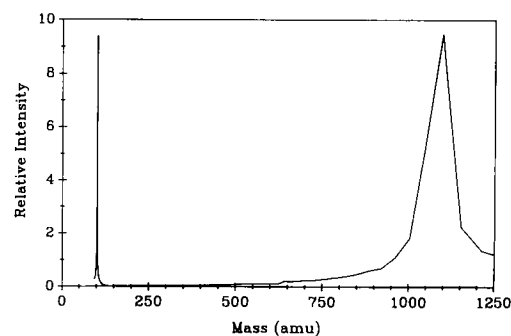

Fig. 8. The simulated mass spectrum for the *m/q* 100 and 1000 ions calculated via Fourier transformation of the collected data (*Y position vs. time*). As predicted, the inhomogeneous electric field has very little effect upon *m/q* 100, however, the large effect upon *m/q* 1000 results in both frequency shifts and loss of resolution.

ACKNOWLEDGEMENTS

REFERENCES

(1) PAUL, W.; REINHARD, H.; VON ZAHN, V.Z. *Physik* 1959, 156,1
(2) BYRNE, J.; FARGO, P.S. *Proc. Phys. Soc. London* 1965, 86,801
(3) BONNER, R.; LAWSON, G; TODD, J.; MARCH, R. *Adv. Mass Spectrom.* 1974, 6, 377
(4) FULFORD, J.; MARCH, R. *Int. J. Mass Spectrom. Ion Phys.* 1978, 26, 155
(5) SOMMER, H.; THOMAS, H.A.; HIPPLE, J.A. *Phys. Rev.* 1949, 76, 1877
(6) ANDERS, L.R.; BEAUCHAMP, J.L.; DUNBAR, R.C., BALDESCHIELER, J.D. *J. Chem. Phys.* 1966, 45, 1062
(7) MCIVER, R.T. *Rev. Sci. Instrum.* 1970, 41, 555
(8) NEUHAUSER, W.; HOHENSTATT, M.; TOSCHEK, P.E.; DEHMELT, H. *Phys. Rev. A* 1980, 22, 1137
(9) ALLISON, J.; STEPNOWSKI, R.M. *Anal. Chem.* 1987, 59, 1072A
(10) PENNING, F.M. *Physica* 1936, 3, 873
(11) ANDERS, L.R.; BEAUCHAMP, J.L.; DUNBAR, R.C.; BALDESCHWIELER, J.D. *J. Chem. Phys.* 1966, 45, 1062.
(12) HUNT, D.F.; SHABANOWITZ, J; YATES, J.R.; ZHU, N.; RUSSELL, D.H.; CASTRO, M.E. *Proc. Natl. Acad. Sci.* 1987, 84, 620.
(13) ALLEMANN, M.; KELLERHALS, H.P.; WANCZEK, K.P. *Int. J. Mass Spectrom. Ion Proc.* 1983, 64, 139.
(14) CASTRO, M.E.; RUSSELL, D.H.; GHADERI, S.; CODY, R.B.; AMSTER, I.J.; MCLAFFERTY, F.W. *Anal. Chem.* 1985, 58, 483.
(15) MARSHALL, A.G. In "*Fourier, Hadamard, and Hilbert Transformations in Chemistry*", Ed by A.G. Marshall, Plenum Publ. Corp., New York, 1982, 136-142.
(16) LAUDE, D.A.; JOHLMAN, C.L.; BROWN, R.S.; WEIL, D.A.; WILKINS, C.L. *Mass Spectrom. Rev.* 1986, 5, 107.
(17) CASTRO, M.E.; RUSSELL, D.H.; GHADERI, S.; CODY, R.B.; AMSTER, I.J.; MCLAFFERTY, F.W. *Anal. Chem.* 1985, 58, 483
(18) LEDFORD, E.B.; GHADERI, S.; WHITE, R.L.; SPENCER, R.B.; KULKARNI, P.S.; WILKINS, C.L.; GROSS, M.L. *Anal. Chem.* 1980, 52, 463.
(19) DUNBAR, R.C.; CHEN, J.H.; HAYS, J.D. *Int. J. Mass Spectrom. Ion Proc.* 1984, 57, 39
(20) SIMION PC/PS2 V4.0 was developed by D.C. McGilvery and modified by D.A. Dahl. The program is distributed by D.A. Dahl, Idaho National Laboratory, Idaho Falls, ID, 1988.
(21) DUNBAR, R.C.; CHEN, J.H.; HAYS, J.D. *Int. J. Mass Spectrom. Ion Proc.* 1984, 57, 39.

(22) BEAUCHAMP, J.L. *J. Chem. Phys.* 1967, 46, 1231

(23) HUNTER, R.L.; SHERMAN, M.G.; MCIVER, R.T. *Int. J. Mass Spectrom. Ion Phys.* 1983, 50, 259.

(24) BARBER, M.; BORDOLI, R.S.; SEDGEWICK, R.D.; TYLER, A.N. *J. Chem. Soc., Chem. Commun.* 1981, 325.

(25) WILKINS, C.L.; YANG, C.L. *Int. J. Mass Spectrom. Ion Proc.*, 1986, 72, 195.

(26) CASTRO, M.E.; RUSSELL, D.H. *Anal. Chem.*, 1984, 56, 578.

(27) HANSON, C.D.; KERLEY, E.L.; CASTRO, M.E.; RUSSELL, D.H. *Anal. Chem.* 1989, 61, 2040.

(28) URAKAWA, J.; SHIBATA, H.; INOUE, M. In *"Ion Cyclotron Resonance Spectrometry"*, K-P. Wanczek, Ed.; 1978, Springer-Verlag, Berlin, pp. 33-58.

(29) GRESE, R.P.; REMPLE, D.L.; GROSS, M.L. In *"Fourier Transform Mass Spectrometry: Evolution, Innovation, and Applications"*, M.V. Buchanan, Ed.; 1988, ACS Symposium Series 359, Chapter 2.

(30) WANG, M.; MARSHALL, A.G. *Anal. Chem.* 1989, 61, 1288

(31) HANSON, C.D.; CASTRO, M.E.; KERLEY, E.L.; RUSSELL, D.H. *Anal. Chem.* 1990, 62, 520.